Pressure Effects on the 4f Electronic Structure of Light Lanthanides

W.-T. Chiu,[1] D. R. Mortensen,[2] M. J. Lipp,[3] G. Resta,[1] C. J. Jia,[4] B. Moritz,[4]
T. P. Devereaux,[4,5] S. Y. Savrasov,[1] G. T. Seidler,[2] and R. T. Scalettar[1]

[1]*Physics Department, University of California, Davis, California 95616, USA*
[2]*Department of Physics, University of Washington, Seattle, Washington 98195-1560, USA*
[3]*Physics Division, Lawrence Livermore National Laboratory, Livermore, California 94550, USA*
[4]*Stanford Institute for Materials and Energy Sciences,*
SLAC National Accelerator Laboratory, Menlo Park, California 94025, USA
[5]*Geballe Laboratory for Advanced Materials, Stanford University, Stanford, California 94305, USA*

(Dated: March 7, 2024)

Using the satellite structure of the $L\gamma_1$ line in non-resonant x-ray emission spectra, we probe the high-pressure evolution of the bare 4f signature of the early light lanthanides at ambient temperature. For Ce and Pr the satellite peak experiences a sudden reduction concurrent with their respective volume collapse (VC) transitions. These new experimental results are supported by calculations using state-of-the-art extended atomic structure codes for Ce and Pr, and also for Nd, which does not exhibit a VC. Our work suggests that changes to the 4f occupation are more consistently associated with evolution of the satellite than is the reduction of the 4f moment. Indeed, we show that in the case of Ce, mixing of a higher atomic angular momentum state, driven by the increased hybridization, acts to obscure the expected satellite reduction. These measurements emphasize the importance of a unified study of a full set of microscopic observables to obtain the most discerning test of the underlying, fundamental f-electron phenomena at high pressures.

arXiv:1708.05460v2 [cond-mat.str-el] 23 Jan 2019

Introduction: The physics and chemistry of lanthanides is of critical importance to fields from catalysis,[1–3], separations chemistry of nuclear waste,[4] to cuprate superconductivity[5, 6] and bioscience.[7, 8] Despite a rich history, theoretical treatment of these materials remains a fundamental challenge. The difficulty stems primarily from the underlying nature of f-electron states. In materials with partially filled f shells, the electrons occupy narrow strongly correlated energy bands. The resulting electronic interactions exist between the well understood atomic and uncorrelated band limits and are responsible for a veritable zoo of exotic behaviors: metal-to-insulator transitions,[9] superconductivity,[10] hidden orderings,[11] etc.

A primary example of the challenges in modeling emergent f-electron phenomena is the volume collapse (VC): at high pressures several lanthanides undergo a first-order phase transition that results in large changes to lattice constants and resistivity.[12, 13] After the discovery of this phenomenon in Ce, [14–16] attention focussed on differentiating the Hubbard-Mott (HM)[17, 18] picture, which considers the increasing interatomic overlap of 4f orbitals with pressure, and Kondo volume collapse (KVC)[19–24] scenario, where the screening of the 4f electrons by broad conduction bands is paramount.

While both HM and KVC theories have had notable successes for Ce, predicting macroscopic observables such as the Ce equation of state, [25, 26] they are distinguished by contrasting expectations for the behavior of a foundational microscopic observable: the presence of a 4f localized electron and related properties such as the magnetic moment. Upon crossing the VC transition, the complete 4f itinerancy predicted by the HM model necessarily extinguishes the 4f moment whereas the hybridization, leading to increased f-screening, of the KVC anticipates smaller effects. A significant step forward was the recognition of similarities, for example in the evolution with pressure of the density of states, between the two viewpoints[23, 27].

Motivated by these observations, Lipp *et al.* presented a study of the pressure evolution of the $L\gamma_1(4d_{3/2} \rightarrow 2p_{1/2})$ non-resonant x-ray emission spectra (NXES) for metallic Ce across its VC.[28] Analogous to the $K\beta'$ feature in 3d-transition metal NXES, the $L\gamma_1$ line exhibits a lower-energy satellite feature, $L\gamma_1'$, arising from (4f, 4d) exchange. As a result, the emission intensity is highly sensitive to the presence of a 4f electron, raising several fundamental unresolved questions concerning the relative importance of the f occupancy and the moment in the evolution of the $L\gamma_1'$ satellite.

Here we report an extension of the Lipp *et al.* work to La, Pr, and Nd trivalent metals which lends further insight into the simultaneous occupation, moment, satellite evolution with hybridization. Specifically, we compare the volume-collapsed NXES data to predictions made by advanced atomic calculations, employing LDA-determined values for the hybridization. The chief conclusion of this paper is that it is the 4f *occupation*, rather than the moment, which more consistently tracks the intensity of the $L\gamma_1'$ satellite. This opens the door to interpretation of NXES spectroscopy of these materials in which the 4f occupation plays a more central role.

Experimental Results: We present the measured $L\gamma_1$ NXES spectra as a function of pressure for La, Ce, Pr, and Nd in Fig. 1. For clarity, the data in Fig. 1(a) has been smoothed using a non-broadening

third-order Savitzky-Golay filter with a 5 eV window (comparable to the lifetime-limited resolution of 3.7-4.0 eV) and normalized to peak intensity. Raw data (without smoothing) is used in Fig. 2 and analysis below. Also shown is the highest pressure data subtracted from lowest pressure for each element, to highlight the influence of pressure on the spectral shape. In Fig. 1(b) we present a quantitative extraction of the relative $L\gamma_1'$ intensities. While comparison to La is a useful diagnostic for Ce as shown above, it does not work well for Pr and Nd where the differences in the multiplet structure of the $L\gamma_1$ peak prevent a direct cross evaluation. Instead we fit the spectrum to a sum of Lorentzians: one to model the contribution from the main peak in the satellite region and the others (two for Pr and three for Nd) to fit the $L\gamma_1'$ peak proper. This procedure has previously been used for Ce NXES.[28] The results shown in Fig. 1(b) reflect the spectral weight of the shoulder relative to the main peak. For Ce, Pr, and Nd these results have been normalized to the largest intensity below the transition for each sample to eliminate small run-to-run variations due to differences in spectrometer tune up that would otherwise prevent direct comparison.

La, which was found to have constant, negligible satellite intensity at all pressures, is left unnormalized. Nd is similarly found to have negligible variation even during the minor change in spectral shape upon the fcc to distorted-fcc transition at 18.0 GPa discussed below. Further measurements are required to determine if Nd eventually undergoes $L\gamma_1'$ reduction, similar to Ce and Pr, upon reaching its delocalized $\alpha - U$ phase at ~ 100 GPa.[29] Before interpreting these results, however, some brief context is needed on known behavior of the light lanthanides under pressure and on the underlying physics of the $L\gamma_1$ NXES spectra.

First, under pressure the lanthanide crystal structures initially pass through several high-symmetry transformations of different stacking sequences of close-packed layers, later transitioning to low-symmetry early-actinide-like phases indicative of f-electron bonding.[30–32] While in Pr this transition is accompanied with a large VC (∼10%), [33–37] Nd reaches its low-symmetry $\alpha - U$ structure entirely through smooth transformations.[29] Hence, Nd does not exhibit a VC transition. Ce is a unique case as it experiences an iso-structural (fcc) VC (15%), unassociated with the high-to-low symmetry transition. For this reason its VC is thought to be primarily electronically-driven.

Second, as demonstrated by Lipp *et al.*, [28] NXES provides a sensitive measure of the evolution of intrinsic 4f signatures in Ce. In $L\gamma_1$ NXES a high-energy photon, tuned well above the $L_2(2p_{1/2})$ edge, promotes a $2p$ electron into the continuum. The resulting core-level vacancy is unstable and may be filled by a $4d_{3/2}$ electron accompanied by either photon emission ($L\gamma_1$ x-ray fluorescence) or Auger electron ejection. When

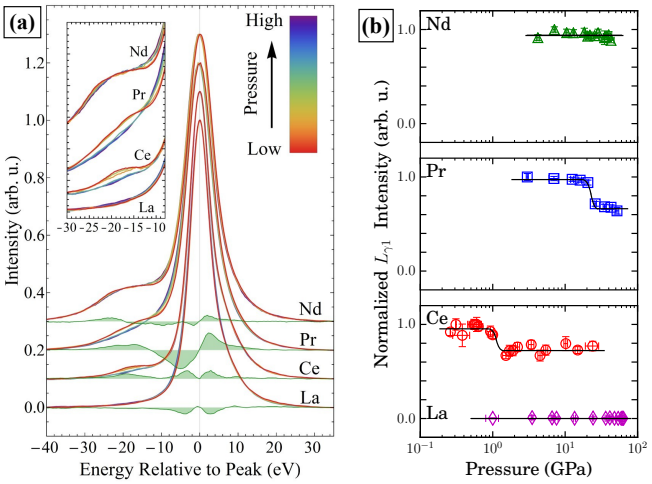


FIG. 1. (Color online.) (a) Experimental $L\gamma_1$ spectra normalized to peak intensity. A non-broadening, third-order Savitzky-Golay smoothing filter of 5-eV window is applied to each spectrum. For clarity, each element has been offset by 0.1. Also shown is the highest pressure data subtracted from the lowest pressure data for each element (shaded green). (b) Experimental intensity of the $L\gamma_1'$ satellite calculated relative to the main $L\gamma_1$ peak. For Ce, Pr, and Nd the intensities have been normalized to the largest value below the transition for each sample in order to reduce the effects of run-to-run variations. La, which has negligible $L\gamma_1'$ intensity, is left unnormalized. The solid black lines are guides for the eye.

the lanthanide species has a nonzero 4f-occupancy, a low energy satellite ($L\gamma_1'$) appears below the main $L\gamma_1$ fluorescence peak due to intra-atomic exchange between 4f and 4d orbitals.[38] The relative intensity and position of the $L\gamma_1'$ shoulder reflects the strength of the coupling and is directly sensitive to the 4f properties.[39, 40]

These observations give rise to a fundamental question: To what extent is the evolution of the satellite a probe of the bare moment or of the occupation? This question complements the well-considered debate concerning whether the VC itself is associated with destruction of the bare moment or its screening. Of course, the moment is linked to the occupation, so the answer is not expected to be completely crisp. In the theoretical work to follow we will compute the satellite peak, occupation, and bare moment as functions of hybridization (pressure) to lend insight into these issues.

With these details in mind, we return to Fig. 1. First, note that the La $L\gamma_1$ NXES spectra show no $L\gamma_1'$ exchange peak up to 64.0±3.0 GPa, beyond the reentrant fcc phase starting at 60 GPa, [43] indicating no change from its nominally $4f^0$ configuration. This null result indicates that the changes observed in Ce, Pr and Nd $L\gamma_1'$ peaks are physically meaningful. That being said, La does display an apparent broadening of the main $L\gamma_1$ peak (on the order of ~ 0.5 eV) with increased pressure. We propose that this effect is due to increased splitting in

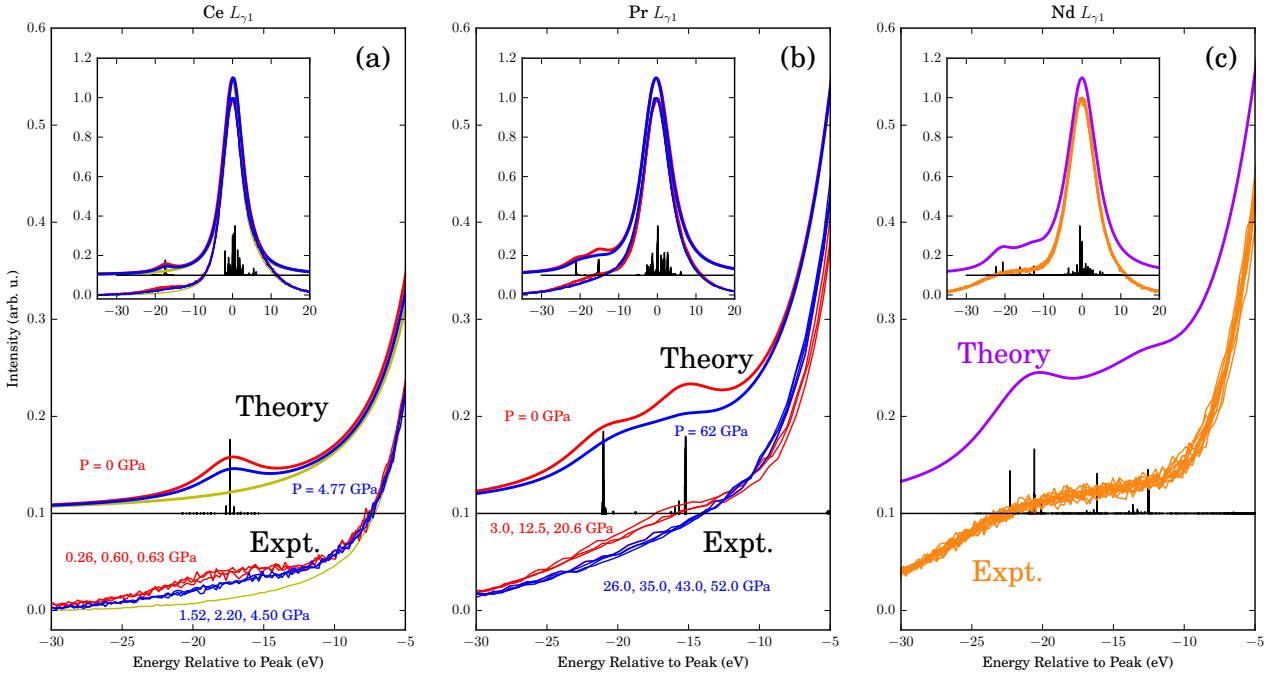


FIG. 2. (Color online.) The shoulder peak (satellite) region of the experimental and calculated X-ray emission spectra for light lanthanide metals. The red(blue) curves are at low(high) pressure. In the theory spectra, low pressure is modeled using parameters at P=0 GPa, and the blue curves are obtained using high pressure parameters. (4.77 GPa for Ce and 62 GPa for Pr.) The yellow curves in (a) are results of lanthanum for a zero shoulder peak reference. (c) The Nd $L\gamma_1$ spectra do not change with pressure up to 43 GPa. Here experimental and theoretical results are shown as orange and purple respectively. The calculated spectra are shifted by +0.1. Insets show the full $L\gamma_1$ spectra. The vertical black lines are the calculated transition probabilities before broadening at zero pressure.

the multiplet structure underlying to the $L\gamma_1$ peak. The changing spectral shape therefore likely contains valuable information on the evolving 4d-electron interactions [44] and thus merits future theoretical consideration.

Second, in contrast to La ($4f^0$), Ce and Pr, which are nominally $4f^1$ and $4f^2$ at ambient conditions, exhibit large and sudden decreases in $L\gamma_1'$ intensity concurrent with the VC transitions (0.9 GPa and 20.0 GPa respectively). Taken naively this result could be used as evidence in support of the HM model as described above. However, it must be noted that although the increased 4f-5d hybridization predicted by KVC invariably mixes the 4f electrons out of their native orbitals, leading to deviations from the ground state electronic configuration; the hybridization causes a rise in the $f^{n\pm1}$ configuration weights at the expense of the sharp, low-pressure f^n configuration. Indeed, this phenomenon has already been experimentally observed in resonant inelastic x-ray scattering measurements for both Ce and Pr. [45, 46] As each configuration carries its own moment, such variations would necessarily modulate the $L\gamma_1'$ feature.

This potentially ambiguous result can be clarified by comparison to La, for which there is a true zero 4f occupancy. The f-electron signature, Fig. 2(a), while reduced, does not fully vanish in the collapsed-phase Ce spectrum, inconsistent with a complete Mott delocalization. Pr NXES, which has a broader main $L\gamma_1$ peak than Ce, does not lend itself to a direct La comparison. The persistence of its 4f hallmark will be demonstrated below.

Nd, which is not subject to any large VC transition, shows a minor change in the $L\gamma_1'$ peak (Fig. 1). There is a shift in $L\gamma_1'$ to a slightly higher energy ($\sim$ 0.3 eV) concomitant with a transition from an fcc to a distorted-fcc structure at $\sim$ 18.0 GPa.[29, 47] As the 4f electrons are still localized at this pressure, the observed shift is likely due to subtle changes in the relative positioning and subsequent electron transfer between conduction subbands which are known to occur during the high-symmetry transformations.[48] As will be shown shortly, however, the normalized amplitude of the $L\gamma_1'$ peak is unchanged during this shift. We note that this change is not associated with any known delocalization transition; for example, prior diffraction and electrical resistivity measurements suggest that 4f delocalization in Nd occurs gradually beginning only at 100 GPa.[48]

Theoretical Predictions and Results: To this point we have made qualitative arguments regarding the pressure dependence of the $L\gamma_1'$ shoulder. We now supplement this with a theoretical treatment. In the Kramers-Heisenberg formalism, the NXES intensity is[49, 50],

$$I_g(\omega) \propto \sum_j \left| \sum_i \frac{\langle j|\hat{T}|i\rangle\langle i|\hat{a_c}|g\rangle}{E_j - E_i - \omega - i\Gamma_i} \right|^2, \qquad (1)$$

where $\hat{T}$ is the dipole operator for $4d \rightarrow 2p$ transitions, $\hat{a_c}$ is the annihilation operator of the core electron, ω is the energy of emission, and $|g\rangle, |i\rangle$ and $|j\rangle$ are the ground, intermediate and final states respectively with energies E_g, E_i and E_j. To account for finite temperature, Eq. 1 is modified assuming a Boltzmann distribution:

$$\langle I(\omega)\rangle_T = \sum_g e^{-E_g/kT} I_g(w) \,/\, \sum_g e^{-E_g/kT} \qquad (2)$$

where T is the working temperature (300 K in the analysis below) and k is the Boltzmann constant.

The electron states are determined by diagonalizing a Hamiltonian combining a single impurity Anderson model [50, 53] with interactions accounting for multiplet terms. The pressure-dependent hybridization V is calculated by a first-principle approach.[54] In Fig. 2, we present the results of these calculations compared to the experimental data. It must be noted that in the theoretical results, the atomic multiplet features composing the $L\gamma_1'$ satellite are sharper than they appear in experiment. This is a consequence of using only five discrete conduction orbitals in place of the true, broad 5d band for hybridization. Such an approximation is necessary to ensure reasonable computation time. Nevertheless, it is clearly demonstrated that the steplike decrease in $L\gamma_1'$ intensity observed in Ce and Pr concomitant with VC is consistent with a sudden increase of 4f-conduction band hybridization as predicted by the KVC model.

The physical observables are calculated by:

$$A_T = \frac{\sum_g e^{-E_g/kT}\langle g|\hat{A}|g\rangle}{\sum_g e^{-E_g/kT}}, \qquad (3)$$

where $\hat{A} = \hat{n_f} = \sum_\nu a^\dagger_{f,\nu} a_{f,\nu}$ for obtaining the 4f occupation number and $\hat{A} = \hat{J}^2$ for the local 4f moment. The values are normalized to zero pressure, as shown in Fig. 3. The results demonstrate that both 4f occupancy and $L\gamma_1'$ intensity decrease as pressure goes up, with the $L\gamma_1'$ intensity doing so at a slightly faster rate. The important point, however, is that a persistent $L\gamma_1'$ feature is indicative of continued 4f localization.

The local moment $\langle J^2\rangle$ behavior is more complicated, since it depends on not only the 4f occupancy but also the occupancy of each j level. Taking Ce first, there are j=5/2 and j=7/2 states with spin-orbit coupling (SOC). The occupancy of the levels will be a function of the 4f on-site energy, ϵ_f and the hybridization V, as shown in Appendix A of [51]. In the V=0 limit, the system follows Hund's rule and only j=5/2 ($\langle J^2\rangle$=8.75) is occupied. As

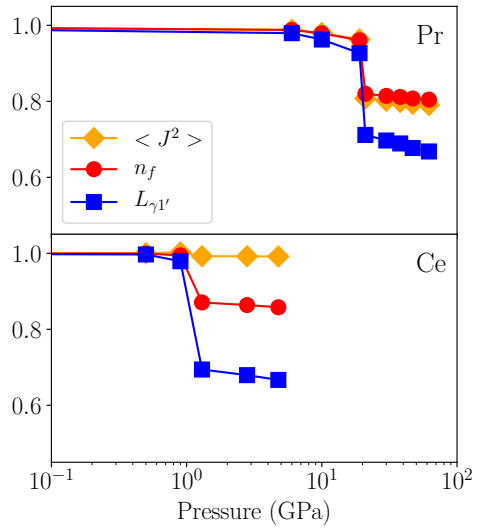


FIG. 3. (Color online.) The calculated bare magnetic moments ($\langle J^2\rangle$), 4f occupation numbers (n_f) and shoulder peak intensities ($L_{\gamma 1'}$) at various pressures for cerium and praseodymium. All quantities are normalized to their zero-pressure value.

V turns on, the occupancy of j=7/2 will grow, and the ratio ($n_{7/2}/n_f$) depends on ϵ_f: When ϵ_f is deep in the valence band the ratio is small, so $\langle J^2\rangle$ decreases as $n_f \sim n_{5/2}$ decreases with rising V; In the other limit, when $n_{7/2}/n_f$ reaches 8/14 at large V, $\langle J^2\rangle$ increases as V goes up.[52] For Ce, $\langle J^2\rangle$, Fig. 3(bottom), the effects from decreasing n_f and increasing $n_{7/2}/n_f$ compensate each other. $\langle J^2\rangle$ stays almost constant as pressure goes up. Ref. [28] reached a similar conclusion concerning the more paramount importance of n_f in tracking the satellite peak, ascribing the (somewhat larger) change reported there in $\langle J^2\rangle$ mostly to the change in occupation, so that the latter is more fundamental. Our conclusions are even somewhat more strong in implicating the occupation, since $\langle J^2\rangle$ is almost completely stable.

Figure 3 (top) similarly emphasizes an abrupt change in $4f$ occupation also occurs through the Pr VC transition, concommitant with the satellite peak evolution. $\langle J^2\rangle$ is also reduced. This is in contrast to results reported for Pr in [52]. The reason is the challenge of considering the full set of rotationally invariant Coulomb interactions within dynamic mean field theory (DMFT). Reference [52] included SOC but only the direct Coulomb interaction. As a result, $\langle J^2\rangle$ for Pr and even Nd behaved similarly to Ce: $\langle J^2\rangle$ increases when volume decreases, because only a higher j=7/2 level is mixed in the ground state as hybridization turns on. We include all interactions, so all multiplet states of Pr mix with the Hund's rule ground state when V is nonzero. In the pressure range of our calculation $\langle J^2\rangle$ drops but retains ~80% of its ambient value across the VC transition. Reproducing the experimental features, both

Ce and Pr $L\gamma_1'$ intensities undergo a large, sudden drop with the VC. These reductions, however, are incomplete with $\sim 70\%$ and $\sim 65\%$ for Ce and Pr respectively.

Conclusion: We have presented a high-quality dataset of high pressure $L\gamma_1$ NXES useful for the characterization of bare 4f electron evolution in the early light lanthanide metals. These data are supported by state-of-the-art modified atomic calculations which extend previous work performed on Ce alone, to Pr and Nd. A central conclusion concerns the evolution of the 4f occupation. There are increasing indications that the most unified picture of the NXES spectra for the light lanthanides and their compounds might be provided by n_f [55, 56] rather than measures of the 4f magnetism- the number of Bohr magnetons, total angular momentum. Our calculations provide crucial evidence of a clear relationship between $L\gamma_1'$ intensity and 4f-conduction band hybridization. Thus, despite the importance of Kondo screening of the moments in the volume collapse of Ce and Pr, the interpretation of their NXES spectra appears also to fit in a broader, common picture focused on 4f occupation.

ACKNOWLEDGEMENTS

NXES studies were performed under the auspices of the US Department of Energy by Lawrence Livermore National Laboratory under Contract No. DE-AC52-07NA27344 and at HPCAT (Sector 16), Advanced Photon Source (APS), Argonne National Laboratory. HPCAT operations are supported by DOE-NNSA under Award No. DE-NA0001974 and DOE-BES under Award No. DE-FG02-99ER45775, with partial instrumentation funding by NSF. The Advanced Photon Source is a U.S. Department of Energy (DOE) Office of Science User Facility operated for the DOE Office of Science by Argonne National Laboratory under Contract No. DE-AC02-06CH11357. The theoretical work of W.-T. C. and R.T.S. was supported by the SSAA program under grant DE-NA0002908. Portions of the computational work were performed using the resources of the National Energy Research Scientific Computing Center supported by the U.S. Department of Energy, Office of Science, under Contract No. DE-AC02-05CH11231. C.J.J., B.M., and T.P.D. at SLAC are supported by the U.S. Department of Energy, Office of Basic Energy Sciences, Materials Sciences and Engineering Division, under Contract No. DE-ACO2-76SF00515 for the atomic multiplet calculations and interpretation. D.R.M. and G.T.S. acknowledge support from the United States Department of Energy, Office of Basic Energy Sciences, under grant DE-SC0002194 and also by the Office of Science, Fusion Energy Sciences, under grant DE-SC0016251. G.R. and S.Y.S. were supported by the US National Science Foundation Grant DMR-1411336 (S.Y.S).

[1] F. T. Edelmann, Chem. Soc. Rev. 41, 7657 (2012).
[2] B. T. Kilbourn, J. Less-Common Metals 126, 101 (1986).
[3] M. Shibasaki and N. Yoshikawa, Chem. Rev. 102, 2187 (2002).
[4] K. Nash and G. Lumetta, *Advanced Separation Techniques for Nuclear Fuel Reprocessing and Radioactive Waste Treatment* (Woodhead Publishing Limited, Cambridge, 2011).
[5] J. G. Bednorz and K. A. Muller, Z. Fur Physik B-Cond. Mat. 64, 189 (1986).
[6] A. L. Ivanovskii, Physics-Uspekhi 51, 1229 (2008).
[7] J. P. Chen, S. Patil, S. Seal and J.F. McGinnis, Nature Nanotech. 1, 142 (2006).
[8] C. Bouzigues, T. Gacoin and A. Alexandrou, Acs Nano 5, 8488 (2011).
[9] M. Imada, A. Fujimori and Y. Tokura, Rev. of Mod. Phys. 70, 1039 (1998).
[10] C. Pfleiderer, Rev. Mod. Phys. 81, 1551 (2009).
[11] P. Chandra, P. Coleman, J.A. Mydosh and V. Tripathi, Nature 417, 831 (2002).
[12] V. S. Egorov and I. N. Khlyustikov, in *Handbook of Physical Quantities*, edited by I. S. Grigoriev and E. Z. Meilikhov (English translation by A. A. Radzig) (CRC, Boca Raton, FL, 1997), pp. 549-572.
[13] N. Velisavljevic, K. M. MacMinn, Y. K. Vohra and S. T. Weir, Appl. Phys. Lett. 84, 927 (2004).
[14] P. W. Bridgman, Proc. of the Amer. Acad. of Arts and Sci. 62, 207 (1927).
[15] P. W. Bridgman, Proc. of the Amer. Acad. of Arts and Sci. 76, 71 (1948).
[16] A. W. Lawson and T.Y. Tang, Phys. Rev. 76, 301 (1949).
[17] B. Johansson, Phil. Mag. 30, 469 (1974).
[18] B. Johansson, Phys. Rev. B11, 2740 (1975).
[19] J. W. Allen and R. M. Martin, Phys. Rev. Lett. 49, 1106 (1982).
[20] M. Lavagna, C. Lacroix and M. Cyrot, Phys. Lett. A 90, 210 (1982).
[21] J. W. Allen and L. Z. Liu, Phys. Rev. B46, 5047 (1992).
[22] A. K. McMahan, K. Held and R. T. Scalettar, Phys. Rev. B67, 075108 (2003).
[23] K. Held, A. K. McMahan and R. T. Scalettar, Phys. Rev. Lett. 87, 276404 (2001).
[24] K. Haule, V. Oudovenko, S.Y. Savrasov and G. Kotliar, Phys. Rev. Lett. 94, 036401 (2005).
[25] M. J. Lipp, D. Jackson, H. Cynn, C. Aracne, W. J. Evans and A. K. McMahan, Phys. Rev. Lett. 101, 165703 (2008).
[26] B. Johansson, A. V. Ruban and I. A. Abrikosov, Phys. Rev. Lett. 102, 189601 (2009).
[27] M. B. Zölfl, I.A. Nekrasov, Th. Pruschke, V. I. Anisimov, and J. Keller, Phys. Rev. Lett. 87, 276403 (2001).
[28] M. J. Lipp, A. P. Sorini, J. Bradley, B. Maddox, K. T. Moore, H. Cynn, T. P. Devereaux, Y. Xiao, P. Chow and W. J. Evans, Phys. Rev. Lett. 109, 195705 (2012).
[29] G. N. Chesnut and Y. K. Vohra, Phys. Rev. B 61, 3768 (2000).
[30] W. B. Holzapfel, J. Alloys and Comp. 223, 170 (1995).
[31] A. K. McMahan, C. Huscroft, R. T. Scalettar and E. L. Pollock, J. Comp.-Aided Mat. Design 5 (1998).
[32] A. Lindbaum, S. Heathman, T. Le Bihan, R. G. Haire, M. Idiri and G. H. Lander, J. Phys.-Cond. Mat. 15, S2297

(2003).
[33] J. S. Olsen, L. Gerward, U. Benedict and J.-P. Itié , Physica 133B, 129(1985).
[34] Y. K. Vohra, S. L. Beaver, J. Akella, C. A. Ruddle and S. T. Weir, J. Appl. Phys. 85, 2451 (1999).
[35] H. K. Mao, R. M. Hazen, P. M. Bell and J. Wittig, J. Appl. Phys. 52, 4572 (1981).
[36] G. S. Smith and J. Akella, J. Appl. Physics 53, 9212 (1982).
[37] B. J. Baer, H. Cynn, V. Iota, C. S. Yoo and G. Y. Shen, Phys. Rev. B 67, 134115 (2003).
[38] P. Glatzel and U. Bergmann, Coord. Chem. Rev. 249, 65 (2005).
[39] K. Jouda, S. Tanaka and O. Aita, J. of Phys.-Cond. Mat. 9, 10789 (1997).
[40] S. Tanaka, H. Ogasawara, K. Okada, and A. Kotani, J. Phys. Soc. Jpn. 64, 2225 (1995).
[41] M. R. MacPherson, G. E. Everett, D. Wohlleben and M. B. Maple, Phys. Rev. Lett. 26, 20 (1971).
[42] T. Naka, T. Matsumoto and N. Mori, Physica B 205, 121 (1995).
[43] F. Porsch and W. B. Holzapfel, Phys. Rev. Lett. 70, 4087 (1993).
[44] F. de Groot, Coord. Chem. Rev. 249, 1-2 (2005).
[45] J. P. Rueff, J. P. Itie, M. Taguchi, C. F. Hague, J. M. Mariot, R. Delaunay, J. P. Kappler and N. Jaouen, Phys. Rev. Lett. 96, 237403 (2006).
[46] J. A. Bradley, K. T. Moore, M. J. Lipp, B. A. Mattern, J. I. Pacold, G.T. Seidler, P. Chow, E. Rod, Y.M. Xiao and W.J. Evans, Phys. Rev. B85, 100102(R) (2012).
[47] J. Akella, S. T. Weir, Y. K. Vohra, H. Prokop, S. A. Catledge and G. N. Chesnut, J. Phys.-Cond. Mat. 11, 6515 (1999).
[48] N. Velisavljevic, Y. K. Vohra and S. T. Weir, High Pressure Res. 25, 137 (2005).
[49] L. J. P. Ament, M. van Veenendaal, T. P. Devereaux, J. P. Hill, and J. van den Brink, Rev. Mod. Phys. 83, 705 (2011).
[50] A. Kotani and S. Shin, Rev. Mod. Phys. 73, 203 (2001).
[51] O. Gunnarsson and K. Schönhammer Phys. Rev. B 28, 4315 (1983).
[52] A. K. McMahan, Phys. Rev. B 72, 115125 (2005).
[53] P. W. Anderson, Phys. Rev. 124, 41 (1961).
[54] See Supplemental Material [url] for experimental and theoretical details, which includes Refs. [28, 31, 33, 37, 40, 45, 57-66].
[55] M. J. Lipp, J. R. Jeffries, H. Cynn, J.-H. Park Klepeis, W. J. Evans, D. R. Mortensen, G. T. Seidler, Y. Xiao, and P. Chow, Phys. Rev. B 93, 064106 (2016).
[56] A. Bianconi, A. Kotani, K. Okada, R. Giorgi, A. Gargano, A. Marcelli, and T. Miyahara, Phys. Rev. B38, 3433 (1988).
[57] S. Heald, G. T. Seidler, D. Mortensen, B. Mattern, J.A. Bradley, N. Hess and M. Bowden, Proc. SPIE, Adv. X-Ray/EUV Optics and Comp. VII 8502, 85020I (2012).
[58] D. R. Mortensen, G.T . Seidler, J. A. Bradley, M. J. Lipp, W. J. Evans, P. Chow, Y. M. Xiao, G. Boman and M. E. Bowden, Rev. Sci. Inst. 84, 083908 (2013).
[59] M. T. Czyżyk and G. A. Sawatzky, Phys. Rev. B 49, 14211 (1994).
[60] R. D. Cowan, *The Theory of Atomic Structure and Spectra.*, (University of California Press, Berkeley, 1981).
[61] O. Gunnarsson, O. K. Andersen, O. Jepsen, and J. Zaanen, Phys. Rev. B 39, 1708 (1989).
[62] M. J. Han, X. Wan, and S. Savrasov, Phys. Rev. B 78, 060401(R) (2008).
[63] J. H. Shim, K. Haule, S. Savrasov, and G. Kotliar, Phys. Rev. Lett. 101, 126403 (2008).
[64] A. Toropova, C. A. Marianetti, K. Haule, and G. Kotliar, Phys. Rev. B 76, 155126 (2007).
[65] K. Haule, C.-H. Yee, and K. Kim, Phys. Rev. B 81, 195107 (2010).
[66] J. R. Schrieffer and P. A. Wolff, Phys. Rev. 149, 491 (1966).

arXiv:1708.05460v2 [cond-mat.str-el] 23 Jan 2019

Supplemental Materials for "Pressure Effects on the 4f Electronic Structure of Light Lanthanides"

EXPERIMENTAL DETAILS

All measurements were performed at beam line 16ID-D of the Advanced Photon Source. Samples (99.9% purity) were loaded into panoramic diamond anvil cells fitted with either 300- 700 μm culet diamonds for lower pressures or 100 μm flat beveled diamonds for higher pressures. To prevent oxide formation each sample was loaded in a glove box flushed with dry nitrogen and brought up to a low pressure to ensure a good seal. Pressure was measured by optical fluorescence from ruby chips loaded with the sample. The incident beam (11.3-20.0 keV) was brought through the diamond with the measured fluorescence escaping perpendicularly through the Be gasket, measured in the scattering plane. La, Pr, and Nd NXES experiments were conducted with newly developed polycapillary-based Bragg spectrometers. [1, 2] These spectrometers use half-lens collimating optics coupled to flat crystal analyzers (Ge 333, Ge 440 and Si 440 for La, Pr, and Nd respectively) with either a scintillation (Cyberstar) or 2D pixel detector (Dectris). All Ce $L\gamma_1$ have been directly reproduced from Lipp *et al.* [3]. All spectra were normalized by incident flux and corrected for a linear background.

THEORY DETAILS

The first piece of the Hamiltonian, whose eigenvalues and eigenvectors determine the NXES intensity, Eq. 1, is an Anderson impurity model,

$$\begin{aligned} H_1 = &\sum_{k,\mu} \epsilon_k a^\dagger_{k,\mu} a_{k,\mu} + \epsilon_f \sum_{\nu} a^\dagger_{f,\nu} a_{f,\nu} \\ &+ \epsilon_p \sum_{\zeta} a^\dagger_{p,\zeta} a_{p,\zeta} + \epsilon_d \sum_{\eta} a^\dagger_{d,\eta} a_{d,\eta} \\ &+ \sum_{k,\nu} V_{f,k} (a^\dagger_{f,\nu} a_{k,\nu} + a^\dagger_{k,\nu} a_{f,\nu}) \\ &+ U_{ff} \sum_{\nu > \nu'} a^\dagger_{f,\nu} a_{f,\nu} a^\dagger_{f,\nu'} a_{f,\nu'} \\ &- U_{fp} \sum_{\nu,\zeta} a^\dagger_{f,\nu} a_{f,\nu} [1 - a^\dagger_{p,\zeta} a_{p,\zeta}] \\ &- U_{fd} \sum_{\nu,\eta} a^\dagger_{f,\nu} a_{f,\nu} [1 - a^\dagger_{d,\eta} a_{d,\eta}]. \end{aligned} \tag{S1}$$

Here ϵ_i is the on-site energy for orbital i, $a_{i\sigma}(a^\dagger_{i\sigma})$ is the annihilation (creation) operator for an electron of orbital angular momentum i, with σ serving as a combined index of the m_l and m_s quantum numbers, U_{ff} is the f-electron Coulomb potential, chosen to take the value U_{ff} = 6 eV. $U_{fp(d)}$ is the 2p (4d) core-hole potential and is set to $U_{fd(p)}$ = 10.5 eV(17.8 eV). We define the energy required to promote a 4f electron to the bottom of conduction orbital to be $E_\Delta(n) = E(|4f^{n-1}5d^1\rangle) - E(|4f^n 5d^0\rangle)$. $E_\Delta(1)$ = 1.3 (0.8) eV[4] for cerium and $E_\Delta(2)$ = 5.3 (4.6) eV for praseodymium below (above) the VC transition. For praseodymium the promotion energy includes double-counting energy.[5] V is the hybridization between the f-electron and conduction orbitals under pressure. For simplicity we took $V_{f,k} = V$. The way V is determined is described below. We assume a 2 eV band width for the five discrete conduction orbitals, with orbitals which span the band evenly.[6] In the absence of hybridization, the ground state consists entirely of the nominal f^n occupation ($n = 1, 2$ for Ce and Pr respectively) as discussed above. As pressure increases across the transition, the ground state becomes a mix of f^n and $f^{n\pm1}$ configurations. We do not consider the $4f^{n+1}$ configuration since the strong 4f-4f coulomb interaction makes the energy of this configuration much higher than the other two configurations- it will not be prominent in the ground state.[4]

The second term, H_2, completes the electron-electron interactions by accounting for multiplet interactions terms:

$$\begin{aligned} H_2 = &\sum_{\nu_1,\nu_2,\nu_3,\nu_4} g_{ff}(\nu_1,\nu_2,\nu_3,\nu_4) a^\dagger_{f,\nu_1} a^\dagger_{f,\nu_2} a_{f,\nu_3} a_{f,\nu_4} \\ &+ \sum_{\nu_1,\nu_2,\zeta_1,\zeta_2} g_{fp}(\nu_1,\zeta_1,\zeta_2,\nu_2) a^\dagger_{f,\nu_1} a^\dagger_{p,\zeta_1} a_{p,\zeta_2} a_{f,\nu_2} \\ &+ \sum_{\nu_1,\nu_2,\eta_1,\eta_2} g_{fd}(\nu_1,\eta_1,\eta_2,\nu_2) a^\dagger_{f,\nu_1} a^\dagger_{d,\eta_1} a_{d,\eta_2} a_{f,\nu_2} \\ &+ \sum_{\nu_1,\nu_2} \alpha_{\nu_1,\nu_2} a^\dagger_{f,\nu_1} a_{f,\nu_2} + \sum_{\zeta_1,\zeta_2} \beta_{\zeta_1,\zeta_2} a^\dagger_{p,\zeta_1} a_{p,\zeta_2} \\ &+ \sum_{\eta_1,\eta_2} \gamma_{\eta_1,\eta_2} a^\dagger_{d,\eta_1} a_{d,\eta_2}. \end{aligned} \tag{S2}$$

where g are the parameters of the Slater-Koster integrals, and α, β and γ are the spin-orbit coupling parameters for respectively the f, p, and d orbitals. All of these values (including the on-site energy ϵ_i) were obtained from Cowan's atomic structure code[7] using the Hartree-Fock approximation and including relativistic effects. The values of g are scaled by 0.8 to account for screening, except for the exchange integrals of 4f and 4d orbitals, $G(4d, 4f)$, which we take 0.72 of the nominal value. The scaling factors are empirical for Ce, Pr, and Nd, and give the correct shoulder peak locations.

To obtain the hybridization matrix elements (V), we calculate the average hybridization function Δ between

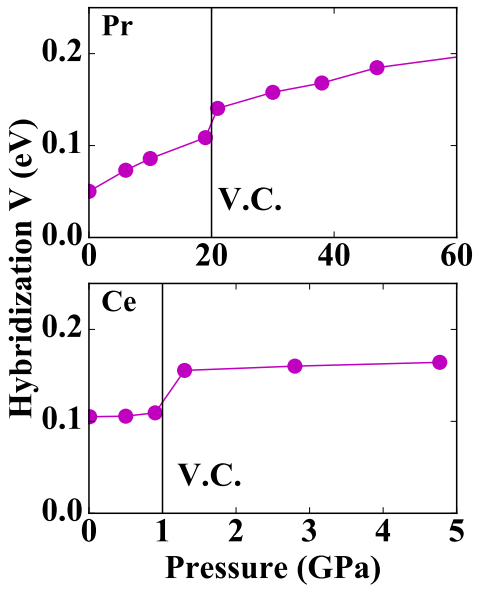


FIG. S1. (Color online)The hybridization V between localized 4f orbitals and conduction bands for cerium and praseodymium as a function of pressure. The vertical black lines indicate roughly the pressures crossing the volume collapse transition at room temperature.

the 4f and the conduction states [8–12]. We first use the software routine developed for DFT+DMFT calculations by Haule *et al.* [12] to compute the hybridization function Δ_τ in the absence of correlation effects (U=J=0) for each atomic site (τ) within the unit cell. For the DFT part of the calculation, a mesh with 5000 k-points within the Brillouin zone, plane-wave cutoff of $R_{MT}K_{max} = 10$ and maximum angular momentum of $L_{MAX} = 12$ were used. All calculations were performed with the Perdew-Burke-Ernzerhof generalized gradient approximation (PBE-GGA) for the exchange-correlation energy and $G_{MAX} = 14$. Spin-orbit coupling was included using an extended energy range of $E_{MIN} = -10.0$ and $E_{MAX} = 10.0$. The lattice constants for the DFT calculation were determined using the relation between volume and pressure for cerium and praseodymium taken from [14–16].

To compute the hybridization function, the routine first projects the DFT eigenstates ($E(\vec{k},n)$, $|\vec{k},n\rangle$) onto the orbital basis for the impurity problem ($|\tau,\nu\rangle$, $\nu = \{j, m_j\}$) and determines the local lattice Green's function, which in diagonal basis is given by,

$$G^{loc}_\tau(\nu;\omega) = \sum_{\vec{k}.n} \frac{\langle\tau,\nu|\vec{k},n\rangle\langle\vec{k},n|\tau,\nu\rangle}{\omega + \mu - E(\vec{k},n) - \Sigma(\vec{k},n;\omega)}, \quad \text{(S3)}$$

where $\Sigma(\vec{k},n;\omega)$ is the DMFT embedded self-energy which in the absence of correlations is zero. The hybridization function $\Delta_\tau(\nu;\omega)$, is then calculated using the DMFT self-consistency condition that the impurity Green's function is equivalent to the local lattice Green's function,

$$\frac{1}{\omega - E^{imp}_\tau(\nu) - \Sigma_\tau(\nu;\omega) - \Delta_\tau(\nu;\omega)} = G^{loc}_\tau(\nu;\omega), \quad \text{(S4)}$$

where $E^{imp}_\tau(\nu)$ are the impurity energy levels and $\Sigma_\tau(\nu;\omega)$ is the self-energy in the orbital basis for the impurity problem which is likewise zero in the absence of correlations. The hybridization function was calculated on the real-axis for each unique atomic site using relativistic harmonics for the orbital basis of the embedded impurity problem. The average hybridization function $\Delta(\nu;E_F)$ was then determined by averaging the hybridization function of all atoms within the unit cell,

$$\Delta(\nu;E_F) = \frac{1}{N}\sum_{\tau=1}^{N}\Delta_\tau(\nu;E_F). \quad \text{(S5)}$$

Finally the hybridization matrix elements (V) are estimated by taking the square root of the imaginary part of the hybridization function at the Fermi energy, E_F, with normalization:[9, 13]

$$|V|^2 = -\frac{1}{\pi} Im \sum_\nu \frac{\Delta(\nu;E_F)}{14 \times N(E_F)}. \quad \text{(S6)}$$

Here $N(E_F)$ is the number of states per atom in a unit cell. Once V is obtained, it can be inserted into the single impurity Anderson model.

[1] S. Heald, G. T. Seidler, D. Mortensen, B. Mattern, J. A. Bradley, N. Hess and M. Bowden, Proc. SPIE, Adv. X-Ray/EUV Optics and Comp. VII 8502, 85020I (2012).

[2] D. R. Mortensen, G. T. Seidler, J. A. Bradley, M. J. Lipp, W. J. Evans, P. Chow, Y. M. Xiao, G. Boman and M. E. Bowden, Rev. Sci. Inst. 84, 083908 (2013).

[3] M. J. Lipp, A. P. Sorini, J. Bradley, B. Maddox, K. . Moore, H. Cynn, T. P. Devereaux, Y. Xiao, P. Chow and W. J. Evans, Phys. Rev. Lett. 109, 195705 (2012).

[4] J. P. Rueff, J. P. Itie, M. Taguchi, C.F. Hague, J. M. Mariot, R. Delaunay, J.P. Kappler and N. Jaouen, Phys. Rev. Lett. 96, 237403 (2006).

[5] M. T. Czyżyk and G. A. Sawatzky, Phys. Rev. B 49, 14211 (1994).

[6] In a study of the X-ray emission spectroscopy of rare-earth oxides, the valence band was approximated by a single level. See S. Tanaka, H. Ogasawara, K. Okada, and A. Kotani, J. Phys. Soc. Jpn. 64, 2225 (1995).

[7] R. D. Cowan, *The Theory of Atomic Structure and Spectra.*, (University of California Press, Berkeley, 1981).

[8] O. Gunnarsson, O. K. Andersen, O. Jepsen, and J. Zaanen, Phys. Rev. B 39, 1708 (1989).

[9] M. J. Han, X. Wan, and S. Savrasov, Phys. Rev. B 78, 060401(R) (2008).

[10] J. H. Shim, K. Haule, S. Savrasov, and G. Kotliar, Phys. Rev. Lett. 101, 126403 (2008).
[11] A. Toropova, C. A. Marianetti, K. Haule, and G. Kotliar, Phys. Rev. B 76, 155126 (2007).
[12] K. Haule, C.-H. Yee, and K. Kim, Phys. Rev. B 81, 195107 (2010).
[13] J. R. Schrieffer and P. A. Wolff, Phys. Rev. 149, 491 (1966).
[14] A. K. McMahan, C. Huscroft, R. T. Scalettar and E. L. Pollock, J. Comp.-Aided Mat. Design 5 (1998).
[15] J. S. Olsen, L. Gerward, U. Benedict and J.-P. Itié , Physica 133B, 129(1985).
[16] B. J. Baer, H. Cynn, V. Iota, C. S. Yoo and G. Y. Shen, Phys. Rev. B 67, 134115 (2003).